IVYSPRING
INTERNATIONAL PUBLISHER

Theranostics

Research Paper

ROS-Responsive Mitochondria-Targeting Blended Nanoparticles: Chemo- and Photodynamic Synergistic Therapy for Lung Cancer with On-Demand Drug Release upon Irradiation with a Single Light Source

Caixia Yue[1,2], Yuming Yang[1], Chunlei Zhang[1], Gabriel Alfranca[1], Shangli Cheng[1], Lijun Ma[3], Yanlei Liu[1,2], Xiao Zhi[1], Jian Ni[1], Weihua Jiang[3], Jie Song[1], Jesús M. de la Fuente[1], and Daxiang Cui[1,4]✉

1. Institute of Nano Biomedicine and Engineering, Key Laboratory for Thin Film and Microfabrication Technology of the Ministry of Education, Shanghai, Engineering Center for Intelligent Diagnosis and Treatment Instrument, Department of Instrument Science & Engineering, School of Electronic Information and Electrical Engineering, Shanghai Jiao Tong University, Shanghai 200240, P. R. China;
2. School of Biomedical Engineering, Shanghai Jiao Tong University, Shanghai 200240, P. R. China;
3. Department of Oncology, Tongren Hospital, Shanghai Jiao Tong University School of Medicine, Shanghai 200336, P. R. China;
4. National Center for Translational Medicine, Collaborative Innovational Center for System Biology, Shanghai Jiao Tong University, Shanghai 200240, P. R. China.

✉ Corresponding author: dxcui@sjtu.edu.cn.

Abstract

Mitochondria in cancer cells maintain a more negative membrane potential than normal cells. Mitochondria are the primary source of cellular reactive oxygen species (ROS), which are necessary for photodynamic therapy. Thus, the strategy of targeting mitochondria can maximize the photodynamic therapeutic efficiency for cancer. Here we report, for the first time, synthesis of a new mitochondria-targeting drug delivery system, ZnPc/CPT-TPPNPs. To synthesize this novel compound, polyethylene glycol was functionalized with thioketal linker-modified camptothecin (TL-CPT) and triphenylphosphonium to form the block copolymer, TL-CPT-PEG$_{1K}$-TPP. The ZnPc/CPT-TPPNPs was constructed for delivery of the photosensitizer Zinc phthalocyanine (ZnPc) by blending the block copolymer TL-CPT-PEG$_{1K}$-TPP with 1, 2-distearoyl-*sn*-glycero-3-phosphoethanolamine-N-[methoxy (polyethylene glycol)] (DSPE-PEG).Triphenylphosphine can accumulate selectively several hundred-fold within mitochondria. The thioketal linker is ROS-responsive and CPT can be released upon ROS cleavage. We also show that the ZnPc loaded in ZnPc/CPT-TPPNPs absorbed the 633 nm laser to produce ROS, which could be utilized both in photodynamic therapy and to cleave the thioketal linker thereby releasing camptothecin for chemotherapy. Thus, the mitochondria-targeting nanoparticles could elevate photodynamic therapeutic efficacy. Our results showed that surface modification of the nanoparticles with triphenylphosphine cations facilitated efficient subcellular delivery of the photosensitizer to mitochondria. The nanoparticles had a good ROS-responsive effect to release CPT, which could transfer to the nucleus and interfere with DNA replication as a topoisomerase I inhibitor. Thus, the blended nanoparticles provide a new promising approach as a mitochondria-targeting ROS-activated chemo- and photodynamic therapy with a single light source for lung cancer.

Key words: mitochondria-targeting nanoparticles, ROS-responsive, Zinc phthalocyanine, photodynamic therapy, camptothecin.

Introduction

Mitochondria are critical subcellular organelle for aerobic respiration and ATP synthesis and are considered as the cellular power source [1]. Mitochondria are also regulators of the intrinsic pathway of apoptosis, which is regarded as the major mode of cell death in cancer therapy [2, 3]. Also, mitochondrial dysfunction has been associated with multiple aspects of tumorigenesis and tumor

progression [4, 5]. Photodynamic therapy involves energy transformation from photonic energy (light) to chemical energy (reactive singlet oxygen) via a photosensitizer. Singlet oxygen ($^1O2$), one type of reactive oxygen species (ROS), is the principal cytotoxic agent in photodynamic therapy [6-8]. Due to the short lifetime (<0.1ms) and small diffusion radius of ROS (<20 nm) in biological systems [9], the photosensitizer should be spatially close to the targeted site of action in photodynamic therapy. Mitochondria are key organelles for respiration and the primary source, approximately up to 90%, of cellular ROS generation [10-12]. Hence, the mitochondria-targeting nanoparticles loaded with photosensitizers can perturb ROS homeostasis and further induce cell apoptosis, which can achieve maximized photodynamic therapeutic efficiency.

The functions of mitochondria in tumors differ greatly from those in normal tissues. Mitochondrial membrane potential ($\Delta\Psi m$) in most cancer cells is higher than that in normal cells [13] and favors the uptake of cationic drugs and nanoparticles in carcinoma cells. Previous studies have proved that a potential difference of approximately 60 mV between normal epithelial cells and carcinoma cells could result in a tenfold uptake difference at 37℃ [14, 15]. Triphenylphosphine, a cationic compound with delocalized positive charge, can selectively accumulate several hundred fold within mitochondria because of the negative potential gradient of the organelle (-120 to -170 mV negative inside; Fig. S1) [16, 17].The plasma membrane potential (-30 to -60 mV negative inside; Fig. S1) also drives the accumulation of these molecules from the extracellular fluid into cells, from where they are concentrated further within mitochondria, with >80% of intracellular cations being present in mitochondria [18]. This selective uptake by mitochondria can greatly increase the efficacy and specificity of molecules designed to interact with mitochondria while also decreasing harmful side reactions [1]. This property has been exploited to deliver fluorescent dyes and therapeutic drugs to mitochondria [19-21]. It has been reported that triphenylphosphine-modified nanoparticles can overcome the resistance of some cancer cells [21, 22]. To construct mitochondria-targeting therapeutic agents, the most common strategy is to load drugs into the mitochondria-targeting moiety surface-modified nanoparticles or to conjugate the moiety with model drugs [15, 20, 21, 23].

To obtain the best therapeutic effect while avoiding negative side effects, a variety of nanomaterials were developed to deliver drugs with controllable/on-demand release properties. Many controllable release methods, such as pH, redox, temperature, enzyme, and light, have been used for drug release [6, 24-28]. However, few reports have focused on the drug controlled release of ROS-responsive. Recent reports revealed that thioketal group can be readily cleaved by ROS inspiring us to explore ROS-responsive drug release [9, 29]. Most of the ROS stimulus is light-activated and can provide the advantage of the precisely controlled release of drugs both in space and time. Cancer cells exhibit greater ROS stress than normal cells, partly due to oncogenic stimulation, which increases metabolic activity and mitochondrial malfunction [4]. However, normal cells, with lower ROS basal stress and reserve, appear to have a higher capacity to fight against additional ROS-generating insults than cancer cells. Therefore, the elevation of ROS around tumor environment can selectively kill cancer cells. Photodynamic therapy has been successfully used in skin diseases in the clinic and further extended to cancers [30-33]. ROS produced by photosensitizers can be used in photodynamic therapy and to cleave thioketal groups to release drugs. Thus, it is possible to develop a platform for combining ROS-responsive chemotherapy and photodynamic therapy with a single light source. Zinc phthalocyanine (ZnPc), a photosensitizer with high singlet oxygen quantum yield, is frequently used for photodynamic therapy [34, 35].

In this study, mitochondria-targeting ZnPc/CPT-TPPNPs were prepared by loading the photosensitizer ZnPc. The ZnPc/CPT-TPPNPs were able to target mitochondria and camptothecin (CPT) release was ROS-responsive. The positive charge of the nanoparticles enabled them to permeate lipid bilayers easily and to accumulate selectively in mitochondria. The efficiency of the ROS-responsive CPT release was detected with ^{1}H-NMR spectrometry and *in vitro* CPT release assays. The mitochondria-targeting nanoparticles could elevate photodynamic therapeutic efficiency for cancer and had a good tumor passive targeting effect *in vivo*. Overall, the resulted ZnPc/CPT-TPPNPs are potential mitochondria-targeting nanoparticles for chemo- and photodynamic therapy of lung cancer.

Materials and methods

Materials

Triphenylphosphine (PPh3), 5-bromopentanoic acid, 3-mercaptopropionic acid, triethylamine (TEA), N-(3- dimethyl aminopropyl)-N'-ethyl carbodiimide hydrochloride (EDCI), 4-dimethylaminopryidine (DMAP) and camptothecin (CPT) were purchased from Aladdin Reagent Co. Ltd. (Shanghai, China).

Hydroxybenzotriazole (HOBT), 2, 4, 6-trichlorobenzoyl chloride, NH_2-PEG_{1K}-NH_2 and Zinc phthalocyanine (ZnPc) were obtained from J&K Chemical Reagent Co. Ltd. (Shanghai, China). DSPE-PEG_{2K}-NH_2 was purchased from Avanti (USA). 2′, 7′-dichlorofluorescein diacetate (DCFH-DA) was purchased from Sigma-Aldrich (USA). Mito-tracker-Green FM dye was supplied by Life Technologies Corporation (California, USA) and JC-1 mitochondrial membrane potential detection assay kit was obtained from Beyotime Biotechnology Co. Ltd. (Nantong, China). Calcein-AM was purchased from Dojindo Molecular Technologies Incorporation (Tokyo, Japan).

Synthesis of ROS-cleavable thioketal linker (TL) and ROS-sensitive camptothecin pro-drug TL-CPT

In a typical reaction, a mixture of anhydrous 3-mercaptopropionic acid (5.2 g, 49.1 mmol) and anhydrous acetone (5.8 g, 98.2 mmol) was saturated with dry hydrogen chloride and stirred at room temperature for 4 h. After the reaction, the flask was stoppered and chilled in an ice-salt mixture until crystallization was complete. The crystals were filtered, washed with hexane and cold water, and the thioketal linker product was acquired after vacuum freeze-dried (78%). ^{1}H NMR (400 MHz, DMSO-d_6) δ: 2.74 (t, 4H), 2.50 (t, 4H), 1.53 (s, 6H).

To synthesize ROS-sensitive camptothecin pro-drug TL-CPT, TL (252.1 mg, 1.0 mmol) was dissolved in anhydrous DMF (5mL). The solution of triethylamine (TEA, 303.6 mg, 3.0 mmol), 2, 4, 6-trichlorobenzoylchloride (241.9 mg, 1.0 mmol), and 4-dimethylaminopryidine (DMAP, 24.4 mg, 0.2 mmol)in anhydrous DMF (5 mL) was added to the above mentioned solution and the resulting solution was stirred at room temperature for 10 min. Next, the solution of camptothecin (174.1 mg, 0.5 mmol) in 10 mL anhydrous DMF was added and the reaction was stirred for 24 h at room temperature. After that, the reaction was quenched with water and extracted with CH_2Cl_2 for 5 times. The combined organic layers were washed with brine for 5 times, dried over Na_2SO_4 and concentrated to the crude product, which was purified by silica gel chromatography (CH_2Cl_2/CH_3OH: from 20:1 to 15:1 and then 10:1 ratio in sequence) to give the desired product (70% yield).^{1}H NMR (400 MHz, DMSO-d_6) δ: 8.67 (s, 1H), 8.08-8.11 (q, 2H), 7.83 (t, 1H), 7.68 (t, 1H), 7.20 (s, 1H), 5.47 (s, 2H), 5.28-5.34 (q, 2H), 2.75-2.88 (m, 4H), 2.66 (t, 2H), 2.38 (t, 2H), 2.10-2.13 (q, 2H), 1.54 (s, 3H), 1.47 (s, 3H), 0.90 (t, 3H).

Conjugating TL-CPT to one terminal of NH_2-PEG_{1K}-NH_2 to generate the product TL-CPT-PEG_{1K}-NH_2

To conjugate TL-CPT to one terminal of NH_2-PEG_{1K}-NH_2, TL-CPT (232.8 mg, 0.4 mmol) was dissolved in anhydrous DMF (10 mL). The solution of triethylamine (TEA, 1.8 mmol), EDCI (134.19 mg, 0.7 mmol) and hydroxybenzotriazole (HOBT, 94.6 mg, 0.7 mmol) in anhydrous DMF (3 mL) was added to the TL-CPT solution and the mixture was stirred at room temperature for 10 min. Next, the solution of NH_2-PEG_{1K}-NH_2 (400mg, 0.4 mmol) in 2 mL of anhydrous DMF was added and the reaction was stirred for 24 h at room temperature. Then, the solution was added dropwise into 100 mL stirred deionized water and stirring was continued for 4 h. Next, the solution was loaded in a dialysis bag (MWCO = 3.5 kDa) and dialyzed against deionized water for 48 h. The purified intermediate TL-CPT-PEG_{1K}-NH_2 (394 mg, 63.0% yield) was lyophilized and stored at -20℃for further use.^{1}H NMR (400 MHz, DMSO-d_6) δ: 8.71 (s,1H), 8.14 (t, 2H), 7.86-7.89 (m, 2H), 7.73 (t, 2H), 7.24 (s, 1H), 5.51 (s, 2H), 5.27-5.33 (q, 2H), 3.40-3.57 (m, 77H), 3.14-3.18 (m, 2H), 2.65-2.83 (m, 4H), 2.29 (t, 2H), 2.13-2.16 (q, 2H), 1.57 (s, 3H), 1.51 (s, 3H), 0.94 (t, 3H).

Synthesis of mitochondria-targeting small molecule PPh_3Br-$(CH_2)_4$-COOH (TPP) and preparation of mitochondria-targeting amphiphilic block copolymer (TL-CPT-PEG_{1K}-TPP)

Synthesis of PPh_3Br-$(CH_2)_4$-COOH: A mixture of 5-bromopentanoic acid (3.1 g, 17.1 mmol) and PPh_3 (4.24 g, 16.1 mmol) in 40 ml of acetonitrile was heated to reflux for 24 h. After completion of the reaction, the mixture was cooled to room temperature. The solvent was then removed by evaporation under pressure. The residue was triturated and added to ethyl acetate, then filtered, and washed with ethyl acetate to give 6.475 g of product as a white solid (91% yield). ^{1}H NMR (400 MHz, DMSO-d_6) δ: 7.53-7.93 (m, 15H), 3.62-3.70 (m, 1H), 3.53 (t, 1H), 2.24-2.32 (m, 2H), 1.53-1.85 (m, 4H).

Synthesis of TL-CPT-PEG_{1K}-TPP: PPh_3Br-$(CH_2)_4$-COOH (291.7 mg, 0.66 mmol) was dissolved in anhydrous DMF (3 mL). The solution of triethylamine (TEA, 2 mmol), EDCI (153 mg, 0.8 mmol), hydroxybenzotriazole (HOBT, 108 mg, 0.8 mmol) in anhydrous DMF(3 mL) was added to the above mentioned solution and the mixture was stirred at room temperature for 10 min. Next, the solution of TL-CPT-PEG_{1K}-NH_2 (200mg, 0.133 mmol) in 4mL of anhydrous DMF was added and the reaction was stirred for 24 h at room temperature. Then, the

solution was added dropwise into 70 mL stirred deionized water and stirring was continued for 4 h. Next, the solution was loaded into a dialysis bag (MWCO = 3.5 kDa) and dialyzed against deionized water for 48 h. The purified intermediate TL-CPT-PEG$_{1K}$-TPP was lyophilized (188.3 mg, 71.2% yield) and stored at -20 °C for further use. ^{1}H NMR (400 MHz, DMSO-d_6) δ: 8.71 (s, 1H), 8.13-8.15 (m, 3H), 7.54-7.78 (m, 14H), 7.40-7.42 (m, 1H), 7.24-7.26 (m, 2H), 5.51 (s, 2H), 5.26-5.38 (q, 2H), 3.38-3.51(m, 81H), 3.15-3.18 (m, 3H), 2.68-2.86 (m, 7H), 2.27-2.29 (m, 2H), 2.11-2.16 (m, 2H), 1.57 (s, 3H), 1.51-1.53 (m, 2H), 1.49 (s, 3H), 1.24 (m, 2H), 0.94 (t, 3H).

Self-assembly of the mitochondria-targeting (ZnPc/CPT-TPPNPs) or mitochondria-non-targeting nanoparticles (ZnPc/CPT-NH₂NPs)

The preparation of ZnPc/CPT-TPPNPs and ZnPc/CPT-NH₂NPs were carried out by a simple sonication method. DSPE-PEG was dissolved in chloroform at a concentration of 50 mg/mL and ZnPc was dissolved in DMSO at a concentration of 0.4 mg/mL. Although the nanoparticles had a different composition, the method of preparation was the same. Take CPT-PEG$_{1K}$-TPP: DSPE (8:1) for example, 8 mg of CPT-PEG$_{1K}$-TPP or CPT-PEG$_{1K}$-NH₂ conjugate were dissolved in 0.1 mL of DMSO. 1 mg DSPE-PEG dissolved in chloroform and 0.4 mg ZnPc dissolved in DMSO were successively added to the solution of CPT-PEG$_{1K}$-TPP or CPT-PEG$_{1K}$-NH₂ and stirred for 1 min at room temperature. The mixture was then added dropwise to deionized water (10 mL) under sonication using an ultrasonic processor at 130 W in an ice bath for 3 min. The solution was centrifuged (5000rpm/min, 3 min) and the sediment was discarded. The supernatant nanoparticles were washed three times using an Amicon ultra-4 centrifugal filter to remove the organic solvent, followed by filtering through a 0.45 μm pore-sized microporous membrane.

The encapsulation efficiency (EE) and drug-loading (DL) were calculated by the following equations:

$$EE\ (\%) = \text{weight of ZnPc in nanoparticles/weight of ZnPc initially added} \times 100\%$$

$$DL\ (\%) = \text{weight of ZnPc in nanoparticles/total weight of nanoparticles} \times 100\%$$

Characterization of nanoparticles

The size and morphology of the ZnPc/CPT-TPPNPs were characterized by BIO-TEM on a Tecnai G2 spirit Biotwin system (FEI, USA). Dynamic light scattering (DLS) measurements were performed using a NiComp380ZLS Zeta Potential/Particle sizer (PSS Nicomp, Santa Barbara, USA). Zeta-potential measurements were carried out on a Malvern Zetasizer Nano ZS90 system. The UV/Vis absorption spectra were measured on a Varian cary 50 UV-VIS spectrophotometer. The fluorescence emission spectra were recorded on a Hitachi FL-4600 spectrofluorometer. ^{1}H NMR spectra were measured on a Bruker Avance Ⅲ 400 MHz spectrometer. Mass spectrometry was performed using ACQUITYTM UPLC & Q-TOF MS Premier system (Waters, USA).

Measurement of the ROS response *in vitro*

The degradation of thioketal linkages in TL-CPT under ROS exposure was investigated by incubating TL-CPT (10.82 μmol of thioketal groups) in a mixture of DMF (0.8 mL) and water (0.2 mL) with H₂O₂ (400 mM) and CuCl₂ (3.2 μM) at 37°C for 48 h. 7 mL of water was added to the solution and the product was precipitated. The product was centrifuged, washed with water twice, and dried in vacuum. The disappearance of the thioketal linkage peak (δ: 1.47, 1.54 ppm) was quantified by[1]H NMR (400 MHz, DMSO-d_6).

In vitro CPT release

The release of CPT from the nanoparticles was studied in a release medium (phosphate buffered saline, PBS, pH 7.4) using a dialysis bag (molecular weight cutoff of 3, 500 Da). The ZnPc/CPT-TPPNPs kept in the dark were used as a control. ZnPc/CPT-TPPNPs or ZnPc/CPT-TPPNPs/ Vitamin C was dissolved in the release media with a power of 50 mW/cm² 633 nm laser irradiation for 30 min. Next, the three groups of nanoparticles were put into the dialysis bags, which were sealed, placed in 20 mL of release medium in centrifuge tubes (50 mL), and incubated at 37℃ in the dark while shaking at 200 rpm. At desired time intervals, 1 mL of the external buffer was removed and replenished with an equal volume of fresh medium. The concentration of CPT in the release medium was then measured by UV-Vis spectra absorption at 360 nm with DMSO added.

Cell culture and cellular ROS detection during irradiation

NCI-H460 human lung cancer cells were acquired from the Cell Bank of Chinese Academy of Science. The cells were maintained at 37 ℃ with 5% CO₂ in RPMI-1640 medium supplemented with 10% FBS, 100 U/mL penicillin, and 0.1mg/mL streptomycin. Before the experiment, the cells were pre-cultured until 75% confluence was reached.

The NCI-H460 cells were incubated with free ZnPc (2.5μg/mL) or ZnPc/CPT-TPPNPs (2.5μg/mL

of free ZnPc equivalent) for 6 h in 12-well plates. 20 µM DCFH-DA was then added and the cells were further incubated for 20 min followed by irradiation using a 633 nm He-Ne laser at a power of 50 mW/cm^2 for 60 s. The cells treated with laser, free ZnPc, ZnPc/CPT-TPPNPs, free ZnPc/laser, and medium only were used as control groups. The intracellular ROS generation was measured by staining cells with DCFH-DA. Subsequently, the fluorescence intensity of DCF inside the cells was detected by flow cytometry.

In vitro cellular mitochondria-targeting uptake

A confocal laser scanning microscope (CLSM) was utilized to detect cellular uptake and distribution of ZnPc/CPT-TPPNPs in NCI-H460 cells. The cells were seeded in 35 mm glass bottom plates and allowed to adhere for 24 h. Subsequently, the medium was replaced with the fresh medium containing ZnPc/CPT-NH$_2$NPs or ZnPc/CPT-TPPNPs (10 µg/mL of free ZnPc equivalent). After 6 h of incubation, the cells were irradiated slightly with 50mW/cm^2 633 nm laser for 20 s and incubated in dark for 2 h. The cells were washed twice with PBS and stained with Mito-Tracker Green FM without fixation with paraformaldehyde. Finally, the cells were examined using the CLSM (Leica TCS SP8, Germany). The excitation wavelength and emission spectrum of each of the fluorescent indicators were as follows: CPT was excited at 406 nm and the fluorescence emission was collected from 420 to 460 nm; Mito-tracker Green FM was excited at 488 nm and the fluorescence emission was collected from 510 to 540 nm; ZnPc was excited at 633nm and emission spectrum was collected from 650 to 800 nm.

For flow cytometry measurements (BD FACS Calibur), NCI-H460 cells (7×10^4 cells per well in 12-well plates) were cultured in particle-free medium for 24 h, and incubated with free ZnPc, ZnPc/CPT-NH$_2$NPs or ZnPc/CPT-TPPNPs (5 µg/mL of free ZnPc equivalent) for additional 2 or 4 h. Subsequently, the cells were washed with PBS twice, trypsinized and resuspended in 0.8 mL of PBS for flow cytometry measurements. 661nm LP channel (FL4) was selected to collect the fluorescence signals.

Flow cytometric analyses of mitochondrial function by JC-1 assay

To evaluate the integrity of mitochondrial functions, we used the cationic dye JC-1 assay. NCI-H460 cells were cultured in 12 well plates at a density of 1x10^5 cells/mL and grown overnight at 37 ℃. Cells were treated with 6.6µg/mL ZnPc, 23µg/mL free CPT, 23µg/mL CPT in ZnPc/CPT-NH$_2$NPs, and 23µg/mL CPT in ZnPc/CPT-TPPNPs for 12 h at 37 ℃.

Cells treated with medium or with the mitochondrial uncoupler, carbonylcyanide-m-chlorophenylhydrazone (CCCP), were used to measure the normal or dissipated membrane potentials. A solution of JC-1 reagent (10 µg/mL in RPMI-1640 medium) was added and incubated for 10 min at 37 °C. The cells were washed for 3 times with PBS, trypsinized, and washed again for 3 times by centrifugation with PBS (1,400 rpm for 4 min at 4 ℃). The resulting cell pellets were resuspended in 500 µL of PBS and analyzed by flow cytometry using 488 nm excitation with 530 nm (FL1 channel) and 585 nm (FL2 channel) bandpass filters.

Cell viability assays

To detect the phototoxicity and chemotherapeutic effects of ZnPc/CPT-TPPNPs, ZnPc/CPT-NH$_2$NPs and free CPT/ZnPc, NCI-H460 cells (5×10^3 cells per well) were seeded in 96-well plates and incubated for 24 h. Then, the culture medium was replaced by 100µL medium containing ZnPc/CPT-TPPNPs, ZnPc/CPT-NH$_2$NPs, or free CPT/ZnPc, followed by incubation for 6 h at 37 °C in dark, and then irradiation with or without a 633 nm laser (50 mW/cm^2) for 3 min. After another 18 h of incubation in the dark, the cell viability was evaluated.

To directly observe the photodynamic therapeutic efficacy, NCI-H460 cells were seeded in 24-well plates (7 x 10^4 cells per well) and incubated for 24 h. The medium was replaced by fresh medium containing ZnPc/CPT-TPPNPs (4 µg/mL of free ZnPc equivalent) or free ZnPc/CPT (4 µg/mL and 14µg/mL) as a control. After 6 h of incubation in the dark, the cells were half-covered and irradiated with 633 nm laser (50 mW/cm^2) for 3 min. After another 2 h of incubation in the dark, the cells were washed with PBS and stained with calcein-AM and propidium iodide (PI).

Xenograft tumor model establishment and biodistribution analyses on tumor-bearing mice

Female BALB/c athymic nude mice (5 weeks old with 16-18 g weight) were purchased from Shanghai Slac Laboratory Animal Co. Ltd (Shanghai, China). All animal experiments were carried out in compliance with the Institutional Animal Care and Use Committee of Shanghai Jiao Tong University. For the establishment of the subcutaneous xenograft tumor models, NCI-H460 cells (1.5×10^6) were administered by subcutaneous injection into the right flanks of the mice.

The tumors were developed for 2 weeks following which the mice were used for *in vivo* imaging and biodistribution analyses. In this

experiment, Chlorin e6 (Ce6) replaced ZnPc as the fluorescent marker. Free Ce6 or Ce6/CPT-TPPNPs (2.5 mg/kg) were intravenously injected into the tail vein of the tumor-bearing mice. The *in vivo* biodistribution and tumor-targeting efficacy of each sample were evaluated by Bruker In-Vivo F-PRO imaging system. Images were taken 1, 3, 5, and 12 h after injection and the nude mice were sacrificed by cervical vertebra dislocation 5 h after injection. Then the tumor and organs including the heart, liver, spleen, lung and kidney were collected and analyzed in the imaging system. Acquisition parameters were: excitation, 630/20 nm; emission, 700/30 nm.

Photodynamic therapy and chemotherapy on tumor-bearing mice

NCI-H460 subcutaneous xenograft tumor models were used for photodynamic therapy and chemotherapy studies. Tumor-bearing mice were used when the volume of tumors reached 50-80 mm^3. The mice were divided into five groups with six mice in each group. The five groups were treated as follows: free CPT and four other groups of PBS, free ZnPc, ZnPc/CPT-NH2NPs, or ZnPc/CPT-TPPNPs each combined with 633 nm laser irradiation. The nanoparticles or control reagent were intravenously injected at doses equivalent to 5 mg/kg of ZnPc and 22.65 mg/kg of CPT. The day of the injection was designated as day 0. Three hours after the injection, some of the tumors were exposed to the 633 nm laser with 50mW/cm^2 for 30 min. The tumor size and body weight of each mouse were recorded. The therapeutic efficacy of the treatments was monitored by measuring the volume of tumors. Tumor volume was determined as (tumor length) *(tumor width)^2/2.

Statistical analysis

Unless otherwise stated, mean±SD values were used for the expression of data. Statistical analyses of data were performed using the Student's *t*-test. Differences of *P*< 0.05 were considered statistically significant.

Results and Discussion

Synthesis and characterization of mitochondria-targeting ROS-sensitive polymer

The mitochondria-targeting ROS-sensitive polymer, TL-CPT-PEG$_{1K}$-TPP, was synthesized as outlined in Fig.1A. ROS-sensitive thioketal linker (TL) was first synthesized by a reaction between the anhydrous 3-mercaptopropionic acid and acetone saturated with dry hydrogen chloride. Subsequently, the TL-CPT was obtained by a reaction between TL and camptothecin (CPT). Finally, TL-CPT was conjugated to one N-terminal group of

NH$_2$-PEG$_{1K}$-NH$_2$ and the mitochondria-targeting cationic triphenylphosphine was conjugated to the other N-terminal group of NH$_2$-PEG$_{1K}$-NH$_2$ in anhydrous N, N-dimethylformamide.

The schematic of the mitochondria-targeting and light-regulated ROS-activated blended nanoparticles is shown in Fig.1B. Because of the mitochondria-targeting ability of the cationic triphenylphosphine, the nanoparticles could localize easily to mitochondria, which favored ROS generation for photodynamic therapy. Once the nanoparticles localized in mitochondria, 633 nm laser irradiation could activate ZnPc to generate ROS for photodynamic therapy. The generated ROS could also quickly cleave the linker that was covalently attached on CPT for specific on-demand drug release. Most of the CPT could transfer to the nucleus to interfere with DNA replication mechanism as a topoisomerase I inhibitor.

The success of the whole synthetic process was verified by ^{1}H NMR spectra and mass spectrometry. In Fig. S2, the peaks of ethyl protons from CPT was ascribed to 0.94 and 2.13-2.16 ppm, the peaks of two methyl protons from TL was shown as 1.51 and 1.57 ppm, and the proton peaks from PEG$_{1K}$was shown as 3.40-3.57 ppm. In Fig. S3, the peaks of aromatic hydrogen protons belonging to triphenylphosphine showed in 7.53-7.93 ppm. In Fig. 2A, except the same peaks as in Fig.S2, the ^{1}H NMR spectrum of TL-CPT-PEG$_{1K}$-TPP had the same peaks of aromatic hydrogen protons as in Fig. S3. ^{1}H NMR spectra also demonstrated the existence of TL and TL-CPT (Fig. S4 and Fig. S5). In addition, the product was further analyzed by mass spectrometry. The mass-to-charge ratio (*m/z*) of 274.9 [M+Na]$^+$ was ascribed to TL (Fig. S6).The mass-to-charge ratio (*m/z*) of 605.1 [M+Na]$^+$ corresponded to ROS-responsive CPT (TL-CPT) and the mass-to-charge ratio (*m/z*) of 363.0 [M]$^+$ belonged to PPh$_3$Br-(CH$_2$)$_4$-COOH (TPP) (Fig. S7 and Fig. S8).

Development of mitochondria-targeting blended nanoparticles and selection of the optimal particle charge and size for mitochondrial uptake

TL-CPT-PEG$_{1K}$-TPP polymers blended with DSPE-PEG-NH$_2$ could self-assemble into nanoparticles with core−shell−corona structure in aqueous media due to their amphiphilic nature. The water insoluble TL-CPT and DSPE chains formed the hydrophobic core, the water-soluble PEG chains served as hydrophilic shell, and TPP formed the mitochondria-targeting corona. To construct ZnPc/CPT-TPPNPs, free ZnPc was incorporated into the blended NPs by a self-assembly procedure with an encapsulation efficiency above 78.6% (Table 1).

Table 1. Characteristics of nanoparticles formulation.

Nanoparticles	Composition[a]	Diameter (nm)[b]	Zeta potential (mV)	PDI	Drug loading (%)[c]	Encapsulation efficiency (%)
ZnPc/CPT-TPPNPs	CPT-PEG$_{1K}$-TPP:DSPE (1:1)	107.6 ± 60.2	28.3 ± 1.8	0.353	4.30 %	86.0%
ZnPc/CPT-TPPNPs	CPT-PEG$_{1K}$-TPP:DSPE (4:1)	92.5 ± 22.1	37.9 ± 0.8	0.144	4.18%	83.6%
ZnPc/CPT-TPPNPs	CPT-PEG$_{1K}$-TPP:DSPE (6:1)	90.3 ± 15.5	39.5 ± 0.7	0.111	4.01%	80.2%
ZnPc/CPT-TPPNPs	CPT-PEG$_{1K}$-TPP:DSPE (8:1)	88.9 ± 8.5	44.9 ± 0.5	0.068	4.27%	85.4%
ZnPc/CPT-TPPNPs	CPT-PEG$_{1K}$-TPP:DSPE (10:1)	77.1 ± 28.5	45.3 ± 1.5	0.269	3.93%	78.6%
ZnPc/CPT-TPPNPs	CPT-PEG$_{1K}$-TPP:DSPE (10:0)	149.4 ± 88.3	23.9 ± 2.2	0.372	3.04%	60.8%
ZnPc/CPT-NH2NPs	CPT-PEG$_{1K}$-NH$_2$:DSPE (8:1)	83.5 ± 17.2	24.0 ± 0.9	0.124	4.38%	87.6%
Ce6/CPT-TPPNPs	CPT-PEG$_{1K}$-NH$_2$:DSPE (8:1)	93.5 ± 28.6	18.5 ± 0.9	0.233	4.52%	83.1%

Diameter, zeta potential, and polydispersity index(PDI) were determined in water by DLS. Data represent mean ± SD.
[a] Composition means weight ratio of CPT-PEG$_{1K}$-TPP:DSPE-PEG or CPT-PEG$_{1K}$-NH$_2$:DSPE-PEG.
[b] SD of the diameter was calculated from the average hydrodynamic diameter by the DLS instrument.
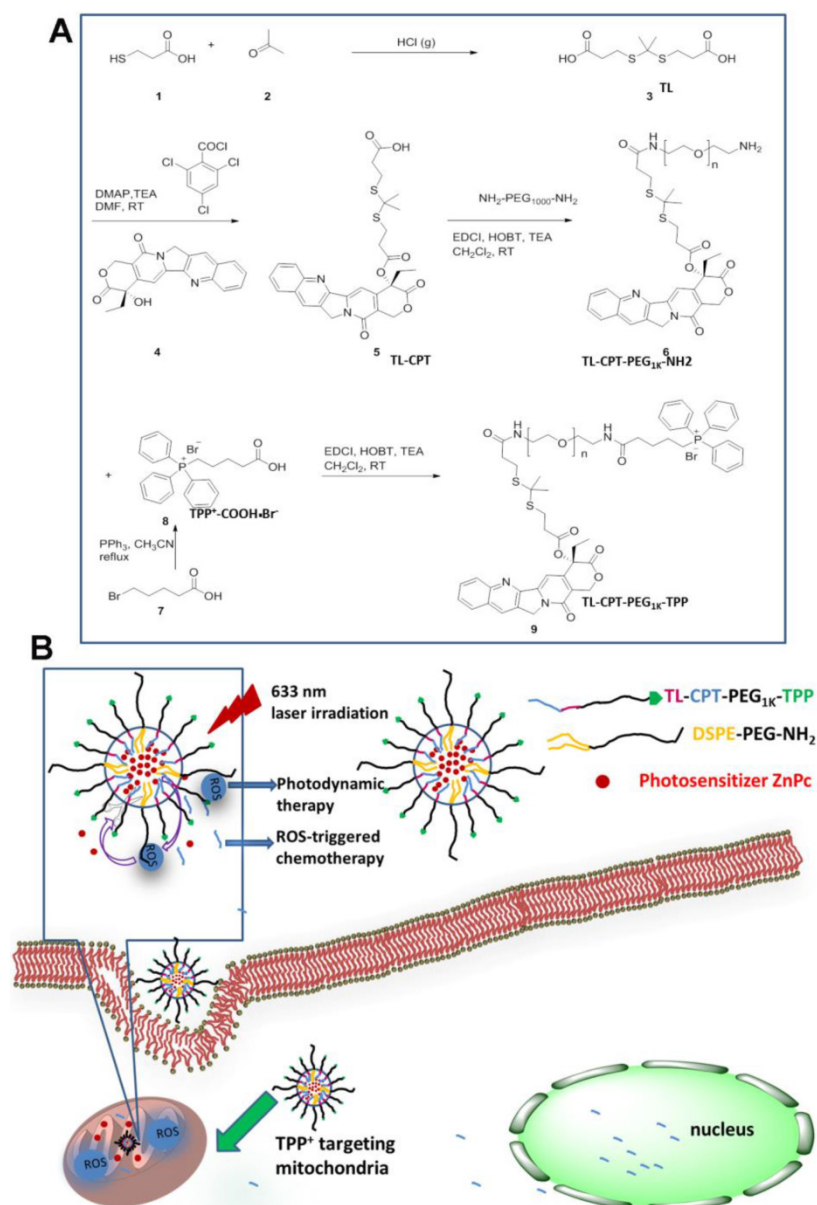[c] Drug loading (%) means the nanoparticles loaded with photosensitizer ZnPc.

Figure 1. Synthesis of the light-regulated, ROS-activated, and mitochondria-targeting ZnPc/CPT-TPPNPs: (A) Synthesis of the ROS-activated, mitochondria-targeting amphiphilic block polymer. Compound 3 is the ROS-cleavable thioketal linker, abbreviated as TL; Compound 5 is the thioketal linker conjugated with camptothecin, abbreviated as TL-CPT; Compound 8 is the mitochondria-targeting molecule, abbreviated as TPP or TPP+COOH•Br- (B) Schematic of the 633 nm light-triggered, ROS-activated and mitochondria-targeting nanoparticles for chemo- and photodynamic combined therapy.

By changing the proportion of TL-CPT-PEG$_{1K}$-TPP in blended nanoparticles, it is possible to modulate the key properties of the nanoparticles, including zeta potential, particle size, and cellular uptake. The optimal application of nanoparticles as mitochondrial-targeting delivery systems requires a high positive charge on their surface. Thus, to choose an optimal formulation, we blended various amounts of TL-CPT-PEG$_{1K}$-TPP with DSPE-PEG-HN$_2$ to construct a library of nanoparticles with varying sizes and surface charges.

ZnPc was loaded into the nanoparticles with various CPT-PEG$_{1K}$-TPP/DSPE ratios and the hydrodynamic diameter was determined by dynamic light scattering (DLS); the nanoparticles ranged in size from 77.1 to 149.4 nm (Table 1).

The addition of some DSPE-PEG could reduce the nanoparticle size. However, accumulation of the nanoparticles can occur in tumors via the enhanced permeability and retention (EPR) effect, which restricted the size of the nanoparticles to no larger than 100 nm for their favorable distribution in the tumor. A positive surface charge favored the nanoparticles to penetrate lipid bilayers for their entry into mitochondria easily. In view of the nanoparticle's formulation from CPT-PEG$_{1K}$-TPP:DSPE-PEG 1:1 to 10:1, the zeta potential of 8:1 and 10:1 formulation had a little change and all the zeta potentials were above positive 44.9 mV. However, the ZnPc/CPT-TPPNPs with 8:1 formulation had the smallest polydispersity index (0.068), which indicated the best homogeneity of the size distribution. Thus, the ZnPc/CPT-TPPNPs with 8:1 formulation and with 44.9 mV zeta potential were chosen as the optimal nanoparticles for mitochondrial uptake and the subsequent studies. The ZnPc/CPT-NH2NPs with CPT-PEG$_{1K}$-NH$_2$/DSPE-PEG (8:1), which did not have cationic triphenylphosphine with the zeta potential of 24 mV, were chosen as control. The amount of CPT in nanoparticles' formulation of TL-CPT-PEG$_{1K}$-TPP:DSPE-PEG with 8:1 ratio was about 14.91% and CPT was about 17.52 percent of the total TL-CPT-PEG$_{1K}$-TPP molecule.

Characterization of the optimal mitochondria-targeting blended ZnPc/CPT-TPPNPs

The aqueous particle size distribution is shown in Fig. 2B. Isolated and uniform spherical ZnPc/CPT-TPPNPs were clearly observed in the Bio-TEM image with the nanoparticle size of about 49 nm (Fig. 2C). The average diameters of the nanoparticles observed by Bio-TEM were smaller than that obtained by DLS. The aqueous particle size, zeta potential, and size distribution are presented in Table 1. The particle size of ZnPc/CPT-TPPNPs remained
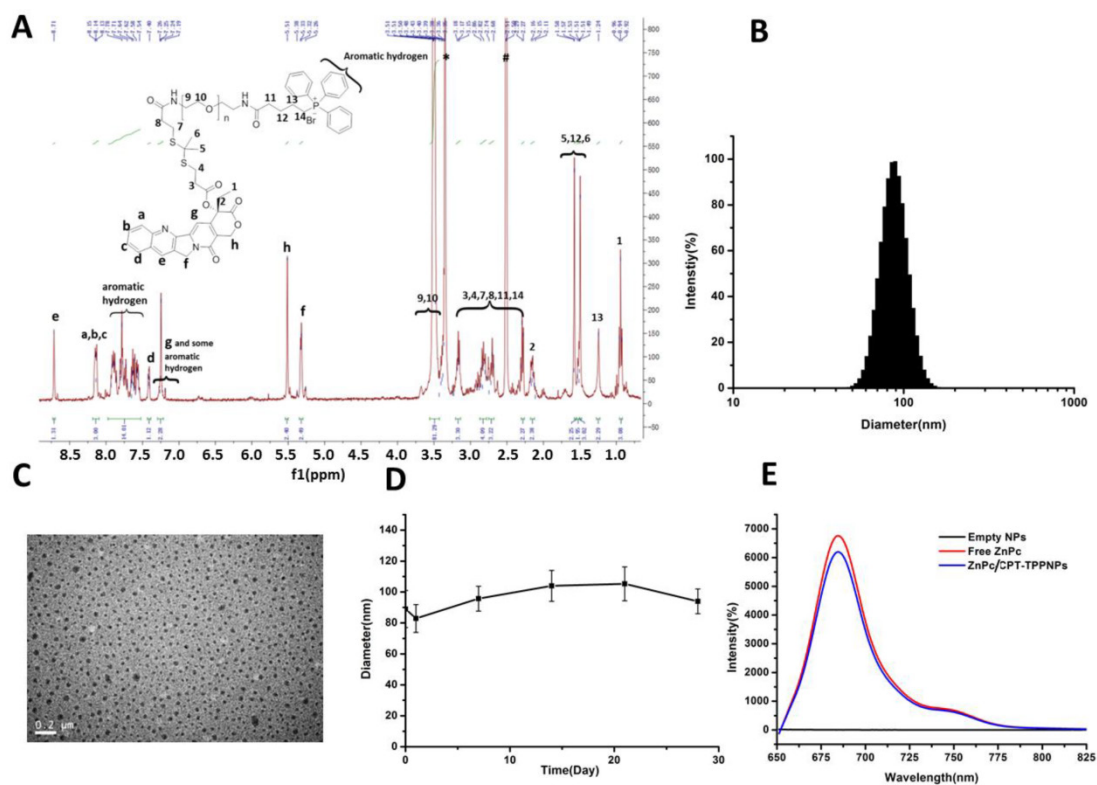

Figure 2. Characteristics of ZnPc/CPT-TPPNPs: (A) ¹H-NMR spectrum of TL-CPT-PEG$_{1K}$-TPP in DMSO-d_6. (B) Size distribution of ZnPc/CPT-TPPNPs by dynamic light scattering (DLS). (C) BIO-TEM of ZnPc/CPT-TPPNPs; the nanoparticle size in TEM was about 49 nm. (D) Colloid stability test of ZnPc/CPT-TPPNPs at 4℃ in water. (E) Fluorescence luminescence spectra of empty NPs, free ZnPc, and ZnPc/CPT-TPPNPs in DMSO; excitation: 630nm.

around the initial particle size without aggregation or precipitation in water for over one month (Fig. 2D), suggesting excellent stability of ZnPc/CPT-TPPNPs. The ZnPc/CPT-TPPNPs showed a fluorescence intensity maximum at $\lambda=684$ nm (Ex: 630 nm, Fig. 2E), whereas empty NPs in DMSO had no absorbance at 650~800 nm. CPT in TL-CPT-PEG$_{1K}$-NH$_2$ had a maximum UV absorbance peak at ~360 nm and the maximum peak of free ZnPc was at ~673 nm in DMSO (Fig. S9C).

ROS-sensitive behavior of thioketal linkages

The degradation of TL-CPT under simulated ROS conditions was quantified by ^{1}H NMR spectroscopy (Fig. 3A). To imitate ROS condition, TL-CPT was incubated with 400 mM H$_2$O$_2$ and 3.2µM CuCl$_2$ at 37℃. The disappearance of the thioketal linkage peak ($\delta=1.47$, 1.54 ppm) confirmed that the thioketal linkages were efficiently cleaved by ROS, generating acetone as a by-product during the cleavage process. This finding was in agreement with a previous study regarding the dethioacetalization using H$_2$O$_2$ [36]. Although a short thiol ligand is attached to CPT after the drug release (Fig.S11 and 12), previous studies demonstrated the ester bond (deriving from thioketal linkage conjugated to CPT) can be hydrolyzed in the lysosomes [37, 38].

As a photosensitizer, ZnPc can produce ROS upon laser irradiation, especially singlet oxygen (^{1}O$_2$) [39]. Since TL-CPT and ZnPc were loaded into the ZnPc/CPT-TPPNPs, it was expected to show ROS-responsive CPT release. ROS produced by ZnPc could cleave the ROS-responsive thioketal linkages for CPT release. To test this idea, we irradiated the ZnPc/CPT-TPPNPs with 633 nm laser before monitoring CPT release. As shown in Fig. 3B, 34% of CPT was released in 4 h. In sharp contrast, ZnPc/CPT-TPPNPs not subjected to light irradiation showed no drug release during the same period. However, drug release was greatly inhibited to 5.3% when vitamin C (VC) was added, probably as a result of the decreased concentration of ROS around the nanoparticles. Thus, there is no premature drug release from ZnPc/CPT-TPPNPs during circulation, but irradiation with light can specifically enhance drug release.
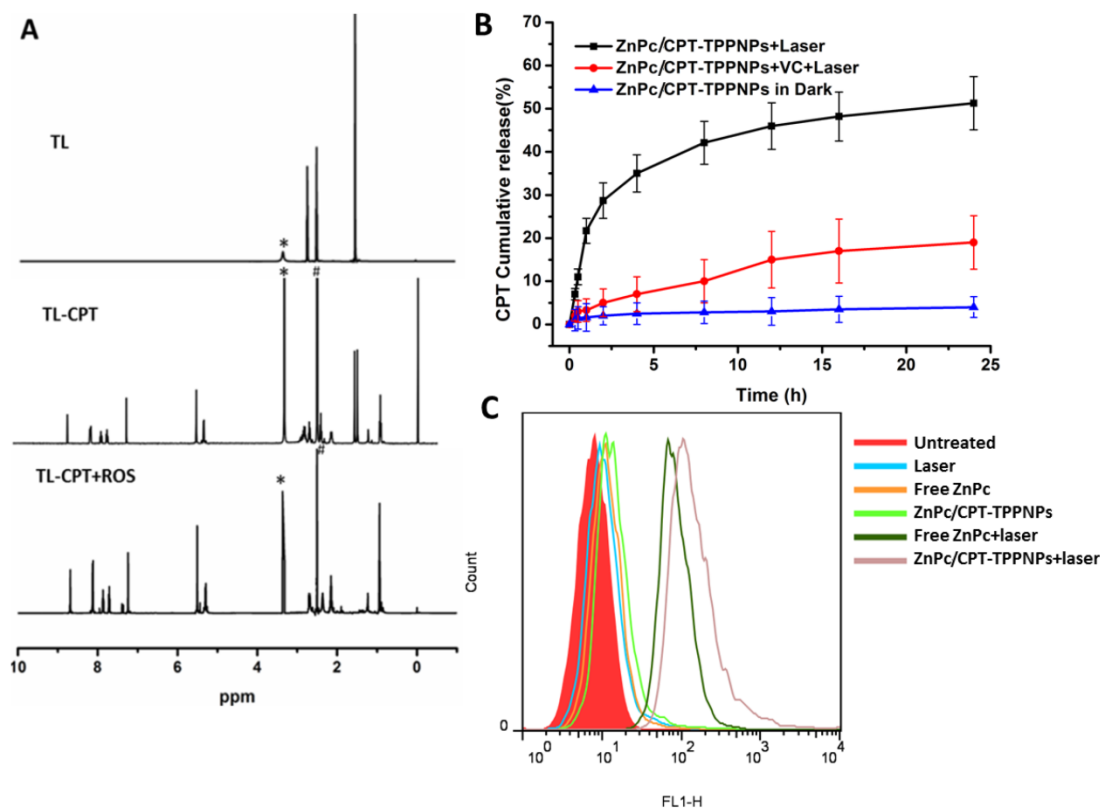

Figure 3. Analysis of sensitivity of thethioketal linker to ROS and generation of ROS by the nanoparticles: (A) Degradation of thioketal linkages in TL-CPT after exposure to ROS as detected by ^{1}H NMR spectroscopy. To imitate ROS conditions, TL-CPT was incubated with 400 mM H$_2$O$_2$ and 3.2 µM CuCl$_2$ at 37℃. (B) Cumulative release profiles of CPT from the nanoparticles with and without light irradiation. Standard deviations are shown as error bars for three parallel experiments. (C) Flow cytometric detection of ROS generation in the presence of DCFH-DA in NCI-H460 cells.

We also examined the intracellular ROS production by ZnPc/CPT-TPPNPs in NCI-H460 cells using the DCFH-DA staining method. DCFH-DA is a nonfluorescent cell-permeable indicator for ROS and becomes fluorescent upon oxidation by ROS after cleavage of the protective acetate groups by intracellular esterases [40]. As anticipated, the ZnPc in ZnPc/CPT-TPPNPs induced the highest amounts of ROS under irradiation which could be detected by flow cytometry (Fig. 3C). The high potency of ZnPc/CPT-TPPNPs correlates with their strong ability to aggregate in mitochondria, which can efficiently increase the level of intracellular ROS in cancer cells.

Evaluation of the cellular uptake and the specific mitochondria-targeting function of the ZnPc/CPT-TPPNPs

After the NCI-H460 cells had been incubated with nanoparticles for 6 h, the cells were irradiated with 50mW/cm^2 633 nm laser and incubated in dark for 2 h. Subsequently, the cells were washed and co-localization of the nanoparticles was examined by confocal microscopy (Fig. 4A). Since the ZnPc/CPT-TPPNPs were designed to target mitochondria, mitochondrial localization was determined by fluorescence dual-staining with a mitochondrial molecular probe, Mito-Tracker Green FM. Green filter (excitation 488 nm, emission 500-540 nm) was used to obtain the signal from Mito-Tracker Green FM. A near infrared filter (excitation 633nm, emission 650-800 nm) was used to obtain signals from ZnPc of the nanoparticles. Compared with untargeted ZnPc/CPT-NH2NPs-treated cells, the cells treated with ZnPc/CPT-TPPNPs showed obvious co-localization between the mitochondrial probe Mito-Tracker Green FM and the photosensitizer ZnPc. The yellow area of the overlapping image represented a co-localization of ZnPc and Mito-Tracker Green FM. These results demonstrated that the ZnPc/CPT-TPPNPs exhibited better selectivity for mitochondria in NCI-H460 cells. After cells were irradiated with 633 nm laser, the ZnPc in mitochondria could generate ROS to cleave the thioketal linker and release CPT. After two additional hours of incubation, the released CPT was transferred to the nucleus. The ZnPc/CPT-TPPNPs-treated cells had a higher proportion of CPT localized in the nucleus compared to ZnPc/CPT-NH2NPs-treated cells.
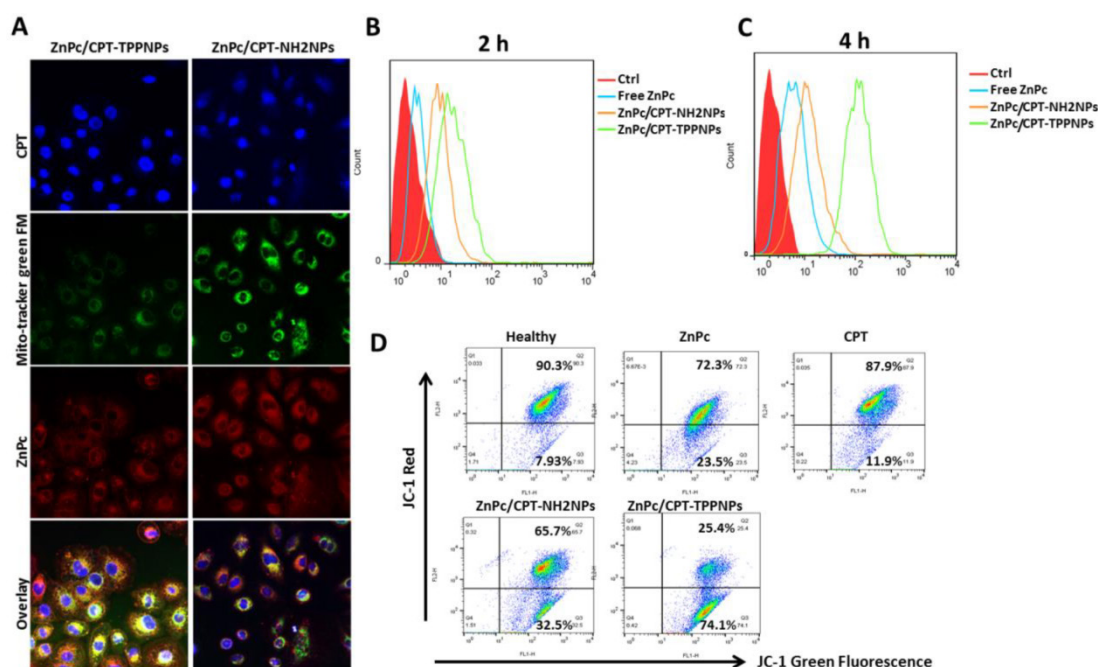

Figure 4. Cellular uptake and mitochondria-targeting ability of ZnPc/CPT-TPPNPs *in vitro*:(A) Confocal microscopy detection of the cellular uptake and mitochondria-targeting ability of ZnPc/CPT-TPPNPs, using Mito-Tracker Green FM. (B) and (C) Flow cytometric analyses of cellular uptake of free ZnPc, untargeted nanoparticles and targeted nanoparticles for 2h and 4h, respectively. (D) Flow cytometric analyses of mitochondrial function by JC-1 assay. Green fluorescence, depolarized mitochondria (J-monomer); red fluorescence, hyperpolarized (J-aggregates). The shift in Δψm was observed by the disappearance of the red-orange-stained mitochondria (large negative mitochondrial membrane potential) and an increase in fluorescent green-stained mitochondria (loss of negative mitochondrial membrane potential).

The results of flow cytometry analysis indicated that triphenylphosphine, as a mitochondria-targeting ligand, could favor cellular uptake (Fig. 4B and C). These results also proved the cellular uptake of positively charged targeted nanoparticles was significantly greater than that of untargeted nanoparticles with different incubation times. After 2 or 4 h incubation, compared with ZnPc/CPT-NH2NPs and free ZnPc, ZnPc/CPT-TPPNPs-treated cells revealed significantly stronger fluorescence intensity, indicating that triphenylphosphine could enhance the cell-penetrating ability of nanoparticles.

We next investigated the mitochondria-targeting function of ZnPc/CPT-TPPNPs on cancer cells with a membrane potential cationic dye, JC-1. This dye exhibits potential-dependent accumulation in the mitochondria accompanied by a fluorescence emission shift from green to red due to the concentration-dependent formation of red fluorescent 'J-aggregates'. The uptake of cationic triphenylphosphine molecules in mitochondria can decrease the membrane potential of mitochondria.
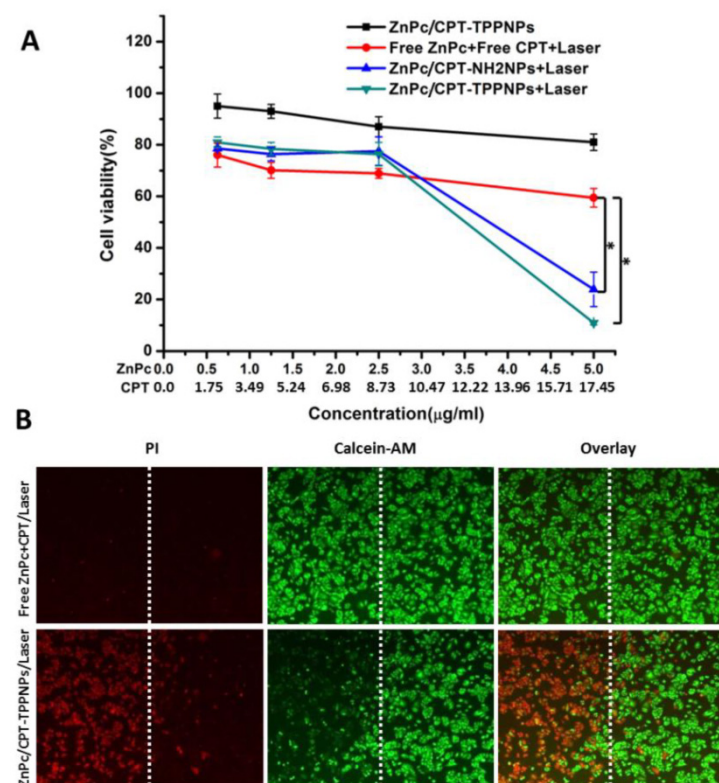

Figure 5. Survival of NCI-H460 cells after chemo- and photodynamic combined therapy: (A) Chemotherapy and photodynamic therapy of the nanoparticles with 633 nm laser. (B) Detection of photodamage of ZnPc/CPT-TPPNPs by fluorescence microscopy using fluorescent probes (double-staining with PI and calcein-AM). Dead cells: red fluorescence of PI; living cells: green fluorescence of calcein-AM. The left side of the dotted line was irradiated with the laser while the right side was in the dark. The data are shown as mean±SD (n =4), * indicates *P*< 0.05.

Thus, we carried out a quantitative analysis of mitochondrial targeting functions in the NCI-H460 cells with flow cytometry (Fig. 4D). The NCI-H460 cells were treated with free ZnPc, free CPT, ZnPc/CPT-NH2NPs, and ZnPc/CPT-TPPNPs. Cells treated with clear medium or mitochondrial uncoupler CCCP were used to measure the normal membrane potential and dissipated membrane potential, respectively. After 12 h of incubation, the cells were stained with JC-1 dye for 10 min. The 'J-monomers' were detected in the green fluorescence channel (FL1) and 'J-aggregates' were detected in the orange-red fluorescence channel (FL2).

As shown in Fig. 4D, the NCI-H460 cells treated with ZnPc/CPT-TPPNPs resulted in an increase in the number of green-fluorescence-positive cells as illustrated in the lower right quadrant of the FACS histogram (74.1%). Under the same conditions, the healthy control NCI-H460 cells only showed a minor green-fluorescence-positive population (7.93%). Compared with ZnPc/CPT-TPPNPs-treated cells, free ZnPc-treated and free CPT-treated cells had fewer green-fluorescence-positive cells, whereas cells treated with free ZnPc or free CPT had 23.5% and 11.9% green-fluorescence-positive cells, respectively. The green-fluorescence of mitochondrial non-targeting ZnPc/CPT-NH2NPs was also lower (32.5%) than that of mitochondrial-targeting ZnPc/CPT-TPPNPs (74.1%). To summarize, these studies indicated that the ability of mitochondria-targeted ZnPc/CPT-TPPNPs to reduce the mitochondrial membrane potential was higher than that of untargeted ZnPc/CPT-NH2NPs.

In vitro chemo- and photodynamic therapy of the ZnPc/CPT-TPPNPs

Mitochondria are key organelles for respiration and the primary source of cellular ROS generation. Hence, the mitochondria-targeting nanoparticles loaded with photosensitizers can achieve maximal photodynamic therapeutic efficiency. To investigate the combined chemo- and photodynamic therapy of ZnPc/CPT-TPPNPs, NCI-H460 cells were treated with ZnPc/CPT-TPPNPs, freeZnPc/CPT/laser, ZnPc/CPT-NH2NPs/laser or ZnPc/CPT-TPPNPs/laser (Fig. 5A). As expected from the quantitative results, the mitochondria-targeting ZnPc/CPT-TPPNPs had little cytotoxicity in dark. Upon 633 nm laser irradiation, compared with free ZnPc/CPT, the cell viability of the ZnPc/CPT-TPPNPs and ZnPc/CPT-NH2NPs

groups dramatically decreased and demonstrated a dose-dependent cytotoxicity. However, the cytotoxicity of ZnPc/CPT-TPPNPs was higher than that of ZnPc/CPT-NH2NPs at the same concentration, because ZnPc/CPT-TPPNPs could be internalized into cells easier than ZnPc/CPT-NH2NPs. The 633 nm laser excited ZnPc to generate ROS, which could be utilized in the photodynamic therapy and also cleaved the ROS-sensitive linker to release CPT. Thus, upon 633 nm laser triggering, ZnPc and CPT had a cumulative effect on lung cancer cells. In conclusion, the nanoparticles could exert synergistic antitumor effects due to the dual functionalities of both phototoxicity and chemotherapy.

To directly observe the photodynamic therapeutic efficacy, the treated cells were stained with calcein-AM and PI (Fig. 5B). Living cells were visualized as green (calcein color) and dead cells were visualized as red (PI color) fluorescence emissions. After 6 h incubation with ZnPc/CPT-TPPNPs in dark, the NCI-H460 cells were half-covered and irradiated with 633 nm laser. Cell death was observed only in the region that was irradiated with the laser while those cells outside the laser region remained viable.

In vivo fluorescence imaging and biodistribution of Ce6/CPT-TPPNPs in a tumor xenograft model

Due to its low fluorescence quantum yield and weak fluorescence [41],ZnPc could not be used for *in vivo* imaging. To acquire *in vivo* biodistribution of the nanoparticles, the blended nanoparticles were loaded with Ce6 instead of ZnPc. The aqueous particle size of Ce6/CPT-TPPNPs was similar to that of ZnPc/CPT-TPPNPs (Table 1). We, therefore, utilized Ce6/CPT-TPPNPs to monitor the biodistribution of the mitochondria-targeting nanoparticles. When the tumor grew for about 2 weeks, free Ce6 or Ce6/CPT-TPPNPs were intravenously injected via tail vein and the time-dependent distribution was monitored by animal fluorescence imaging. As indicated in Fig. 6A, a large number of Ce6/CPT-TPPNPs were located in the liver and tumor 1 h after injection. The Ce6 fluorescence signal of Ce6/CPT-TPPNPs was still strong both in the tumor and liver 3 and 5 h post-injection. The presence of nanoparticles in the liver can be explained by the fact that the Ce6/CPT-TPPNPs are metabolized through the liver where they are taken up and degraded by the Kupffer cells. When the excised tissues of 5 h post-injection were analyzed, tumor tissues from theCe6/CPT-TPPNPs-treated mice showed stronger fluorescence intensity than those

treated with free Ce6 (Fig. 6B and C). The nanoparticles were around 100 nm thereby maximizing the EPR effect at the tumor site.

In vivo chemo- and photodynamic therapy on tumor-bearing mice

To evaluate the chemo- and photodynamic therapeutic efficacy of ZnPc/CPT-TPPNPs *in vivo*, one single dose of PBS, free CPT, free ZnPc, ZnPc/CPT-NH2NPs or ZnPc/CPT-TPPNPs was injected into tumor-bearing mice when the tumor size grew to 50–80 mm^3. After 3 h post-injection, the mice treated with PBS, free ZnPc, ZnPc/CPT-NH2NPs, or ZnPc/CPT-TPPNPs were irradiated at the tumor site with 633 nm laser for 30 min. As shown in Fig. 7A and B, the tumors treated with PBS plus laser irradiation grew rapidly, suggesting the NCI-H460 tumor growth was not affected by the laser irradiation. The growth of NCI-H460 tumors was slightly inhibited by free CPT or by free ZnPc upon laser irradiation. Although CPT is a well-known chemotherapeutic agent for tumor treatment, it usually requires multiple and high dosages to achieve a satisfactory anticancer effect. The treatment of free ZnPc plus laser irradiation could partly inhibit tumor growth, which could be attributed to an insufficient accumulation of the photosensitizer at the tumor site. A single injection of ZnPc/CPT-NH2NPs or ZnPc/CPT-TPPNPs together with the laser irradiation, on the other hand, led to complete eradication of NCI-H460 tumors, leaving the original tumor site with black scars that healed about 3 weeks later. No tumor recurrence was observed in these groups over a course of 50 days. ZnPc could absorb the 633 nm laser to release sufficient ROS, which could then cleave the thioketal linker to release CPT for simultaneous chemotherapy and phototoxicity in tumor tissues. We further investigated the potential toxic side effects of Ce6/CPT-TPPNPs on NCI-H460 tumor-bearing mice. Reduction in the body weight was considered as an indicator for treatment-induced toxicity. A slight reduction in the body weight was noticed after Ce6/CPT-TPPNPs and Ce6/CPT-NH2NPs plus laser treatment (Fig. 7C), which returned to normal 3 weeks later. The mice treated with Ce6/CPT-TPPNPs were sacrificed 50 days later and the major organs of the mice were excised and subjected to H&E staining. No abnormality was observed in the heart, liver, spleen, lung and kidney tissue slices compared with the tissue slices from healthy mice (Fig.S10). These data suggested that the combined chemo- and photodynamic therapy with a single-dose treatment did not cause significant adverse effects *in vivo*.
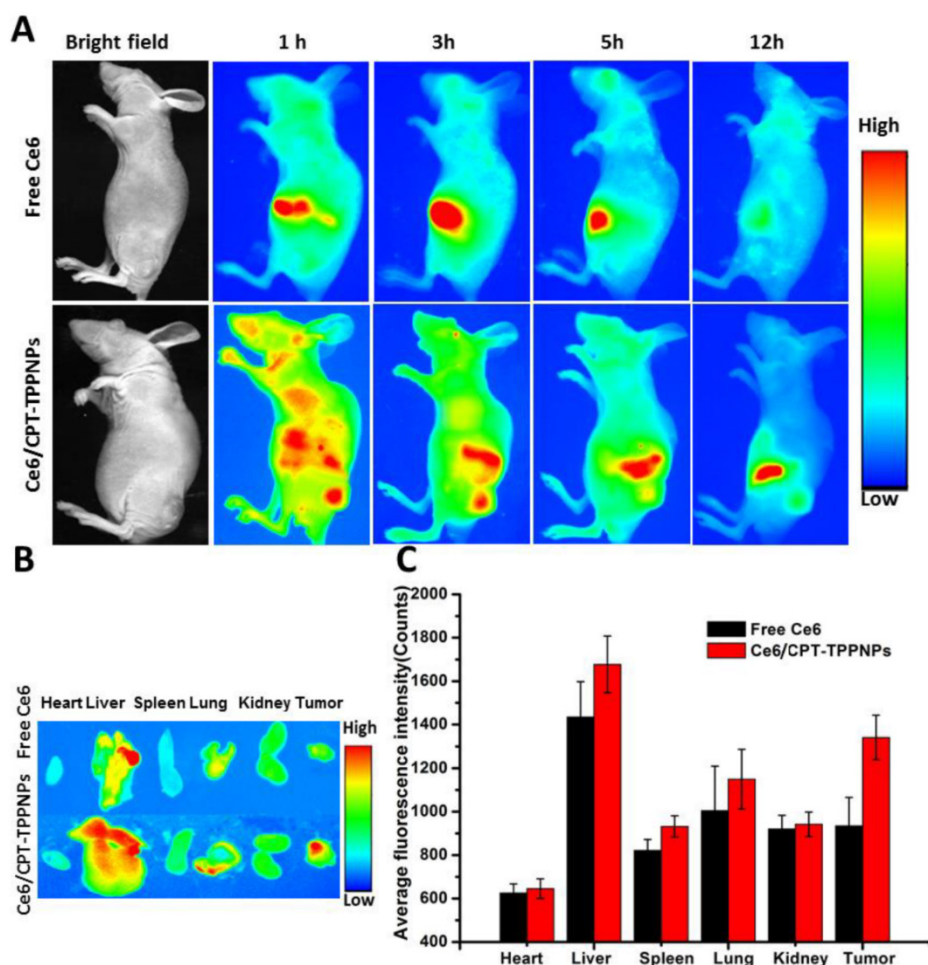
Figure 6. *In vivo* biodistribution analysis on nude mice bearing NCI-H460 tumors after tail vein injection of Ce6/CPT-TPPNPs: (A) Time-lapse fluorescence images of nude mice. (B) Fluorescence images of excised major organs and tumors after injection of Ce6/CPT-TPPNPs or free Ce6 at 5 h. (C) Semiquantitativebiodistribution of free Ce6 or Ce6/CPT-TPPNPs in nude mice determined by the average Ce6 fluoresence intensity of organs 5 h post-injection. The data are shown as mean±SD.
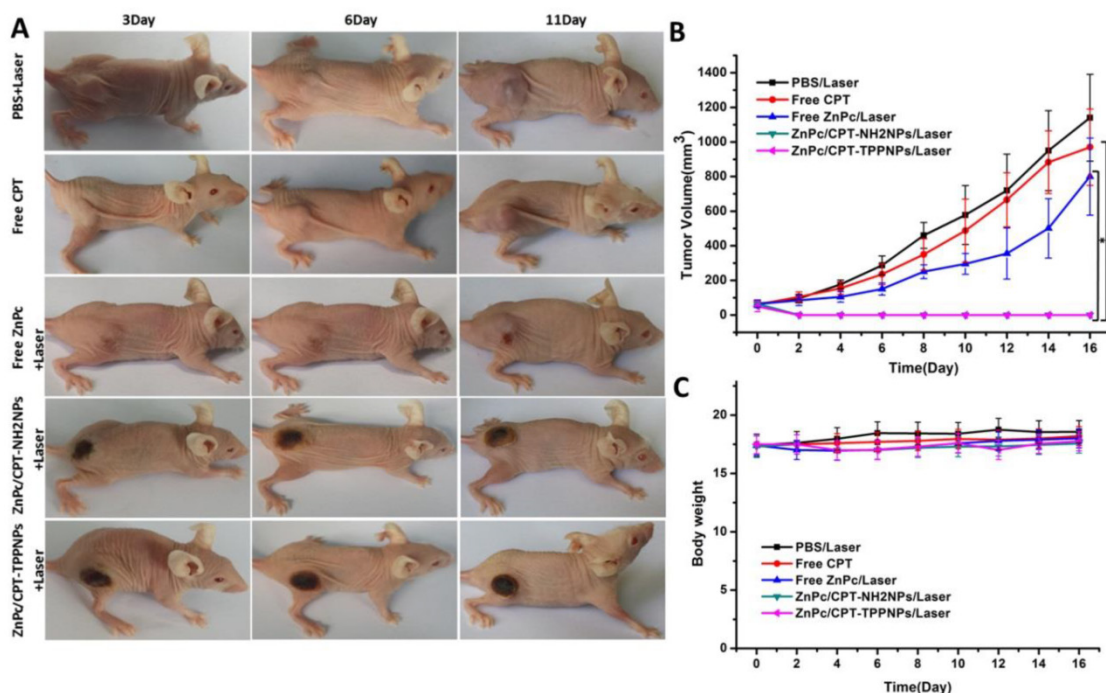

Figure 7. *In vivo* chemo- and photodynamic therapy of the ZnPc/CPT-TPPNPs: (A) Images of mice bearing NCI-H460 tumors after treatment. The mice were irradiated by 633 nm laser with the power density of 50mW/cm2 for 30 min. (B) Growth curves of NCI-H460 tumors in different groups after treatments. (C) Body weight curves after various treatments as indicated. The data are shown as mean±SD (n = 6), * indicates *P*< 0.05.

Conclusion

In this study, mitochondria-targeting cationic ZnPc/CPT-TPPNPs were prepared by loading the photosensitizer ZnPc into the blended drug delivery system containing TL-CPT-PEG$_{1K}$-TPP with DSPE-PEG. The ZnPc/CPT-TPPNPs were able to target mitochondria. The accumulation of nanoparticles in mitochondria decreased the mitochondrial membrane potential. Upon irradiation, the photosensitizer ZnPc triggered ROS-induced cleavage of the thioketal linker releasing CPT. In a xenograft model, the nanoparticles were able to achieve a 633 nm laser-triggered, ROS-activated combined chemo- and photodynamic therapy markedly inhibiting the growth of lung cancer. The dynamic biodistribution analysis indicated that the nanoparticles could gather in the tumor site highly efficiently by the EPR effect and release CPT after exposure to ROS. The nanoparticles exhibited good biocompatibility and did not have significant adverse effects compared with other nanoparticles. To our knowledge, this is the first report demonstrating the high performance of organelle-targeted ZnPc/CPT-TPPNPs exhibiting great potential for a single light source-triggered, ROS-activated combined chemo- and photodynamic therapy for cancer treatment.

Abbreviations

ROS: reactive oxygen species; TL-CPT: thioketal linker-modified camptothecin; ZnPc: Zinc phthalocyanine; DSPE-PEG: 1,2-distearoyl-sn-glycero-3-phosphoethanolamine-N-[methoxy (polyethylene glycol)]; DCFH-DA: 2',7'-dichlorofluorescein diacetate; DMF: N,N-dimethylformamide; CCCP: carbonylcyanide-m-chlorophenylhydrazone; PI: propidium Iodide; Ce6: Chlorin e6.

Supplementary Material

Supplementary figures.
http://www.thno.org/v06p2352s1.pdf

Acknowledgements

Competing Interests

The authors have declared that no competing interest exists.

References

[1] Murphy MP, Smith RAJ. Drug delivery to mitochondria: the key to mitochondrial medicine. Adv Drug Deliver Rev. 2000;41:235-50.
[2] Aronis A, Melendez JA, Golan O, Shilo S, Dicter N, Tirosh O. Potentiation of Fas-mediated apoptosis by attenuated production of mitochondria-derived reactive oxygen species. Cell Death Differ. 2003;10:335-44.
[3] Green DR, Reed JC. Mitochondria and apoptosis. Science. 1998;281:1309-12.
[4] Trachootham D, Alexandre J, Huang P. Targeting cancer cells by ROS-mediated mechanisms: a radical therapeutic approach? Nat Rev Drug Discov. 2009;8:579-91.
[5] Gogvadze V. Targeting mitochondria in fighting cancer. Curr Pharm Des. 2011;17:4034-46.
[6] Liu P, Yue CX, Sheng ZH, Gao GH, Li MX, Yi HQ, et al. Photosensitizer-conjugated redox-responsive dextran theranostic nanoparticles for near-infrared cancer imaging and photodynamic therapy. Polym Chem-Uk. 2014;5:874-81.
[7] Chen Q, Wang X, Wang C, Feng L, Li Y, Liu Z. Drug-induced self-assembly of modified albumins as nano-theranostics for tumor-targeted combination therapy. Acs Nano. 2015; 9:5223-33.
[8] Chen Q, Wang C, Cheng L, He W, Cheng Z, Liu Z. Protein modified upconversion nanoparticles for imaging-guided combined photothermal and photodynamic therapy. Biomaterials. 2014;35:2915-23.
[9] Yuan YY, Liu J, Liu B. Conjugated-polyelectrolyte-based polyprodrug: targeted and image-guided photodynamic and chemotherapy with on-demand drug release upon irradiation with a single light source. Angew Chem Int Edit. 2014;53:7163-8.
[10] Balaban RS, Nemoto S, Finkel T. Mitochondria, oxidants, and aging. Cell. 2005;120:483-95.
[11] Hoye AT, Davoren JE, Wipf P, Fink MP, Kagan VE. Targeting mitochondria. Accounts of chemical research. 2008;41:87-97.
[12] Yu Z, Sun Q, Pan W, Li N, Tang B. A near-infrared triggered nanophotosensitizer inducing domino effect on mitochondrial reactive oxygen species burst for cancer therapy. Acs Nano. 2015; 9:11064-74..
[13] Summerhayes IC, Lampidis TJ, Bernal SD, Nadakavukaren JJ, Nadakavukaren KK, Shepherd EL, et al. Unusual retention of rhodamine 123 by mitochondria in muscle and carcinoma cells. Proc Natl Acad Sci U S A. 1982;79:5292-6.
[14] Modica-Napolitano JS, Aprille JR. Delocalized lipophilic cations selectively target the mitochondria of carcinoma cells. Adv Drug Deliver Rev. 2001;49:63-70.
[15] Hu Q, Gao M, Feng G, Liu B. Mitochondria-targeted cancer therapy using a light-up probe with aggregation-induced-emission characteristics. Angewandte Chemie International Edition. 2014;53:14225-9.
[16] Murphy MP. Selective targeting of bioactive compounds to mitochondria. Trends Biotechnol. 1997;15:326-30.
[17] Smith RA, Porteous CM, Gane AM, Murphy MP. Delivery of bioactive molecules to mitochondria in vivo. Proc Natl Acad Sci U S A. 2003;100:5407-12.
[18] Burns RJ, Murphy MP. Labeling of mitochondrial proteins in living cells by the thiol probe thiobutyltriphenylphosphonium bromide. Arch Biochem Biophys. 1997;339:33-9.
[19] Luo GF, Chen WH, Liu Y, Lei Q, Zhuo RX, Zhang XZ. Multifunctional enveloped mesoporous silica nanoparticles for subcellular co-delivery of drug and therapeutic peptide. Sci Rep. 2014;4:6064.
[20] Marrache S, Dhar S. Engineering of blended nanoparticle platform for delivery of mitochondria-acting therapeutics. Proc Natl Acad Sci U S A. 2012;109:16288-93.
[21] Marrache S, Pathak RK, Dhar S. Detouring of cisplatin to access mitochondrial genome for overcoming resistance. P Natl Acad Sci USA. 2014;111:10444-9.
[22] Solomon MA, Shah AA, D'Souza GGM. In vitro assessment of the utility of stearyl triphenyl phosphonium modified liposomes in overcoming the resistance of ovarian carcinoma Ovcar-3 cells to paclitaxel. Mitochondrion. 2013;13:464-72.
[23] Cho DY, Cho H, Kwon K, Yu M, Lee E, Huh KM, et al. Triphenylphosphonium-conjugated poly (ε-caprolactone)-based self-assembled nanostructures as nanosized drugs and drug delivery carriers for mitochondria-targeting synergistic anticancer drug delivery. Advanced Functional Materials. 2015;25:5479-91.
[24] Dong Y, Yang J, Liu H, Wang T, Tang S, Zhang J, et al. Site-specific drug-releasing polypeptide nanocarriers based on dual-pH response for enhanced therapeutic efficacy against drug-resistant tumors. Theranostics. 2015;5:890-904.
[25] Roy D, Brooks WLA, Sumerlin BS. New directions in thermoresponsive polymers. Chem Soc Rev. 2013;42:7214-43.
[26] Li N, Li N, Yi QY, Luo K, Guo CH, Pan DY, et al. Amphiphilic peptide dendritic copolymer-doxorubicin nanoscale conjugate self-assembled to enzyme-responsive anti-cancer agent. Biomaterials. 2014;35:9529-45.

[27] Chen LF, Wang WQ, Su B, Wen YQ, Li CB, Zhou YB, et al. A light-responsive release platform by controlling the wetting behavior of hydrophobic surface. Acs Nano. 2014;8:744-51.

[28] Fomina N, Sankaranarayanan J, Almutairi A. Photochemical mechanisms of light-triggered release from nanocarriers. Adv Drug Deliver Rev. 2012;64:1005-20.

[29] Shim MS, Xia YN. A reactive oxygen species (ROS)-responsive polymer for safe, efficient, and targeted gene delivery in cancer cells. Angew Chem Int Edit. 2013;52:6926-9.

[30] Wagner A, Denzer UW, Neureiter D, Kiesslich T, Puespoeck A, Rauws EA, et al. Temoporfin improves efficacy of photodynamic therapy in advanced biliary tract carcinoma: A multicenter prospective phase II study. Hepatology. 2015;62:1456-65.

[31] Choudhary S, Nouri K, Elsaie ML. Photodynamic therapy in dermatology: a review. Laser Med Sci. 2009;24:971-80.

[32] Gao J, Liu M, Zou Y, Mao M, Shen T, Zhang C, et al. Long non-coding RNA growth arrest-specific transcript 5 is involved in ovarian cancer cell apoptosis through the mitochondria-mediated apoptosis pathway. Oncol Rep. 2015;34:3212-21.

[33] Wang C, Sun X, Cheng L, Yin S, Yang G, Li Y, et al. Multifunctional theranostic red blood cells for magnetic-field-enhanced in vivo combination therapy of cancer. Advanced Materials. 2014;26:4794-802.

[34] Josefsen LB, Boyle RW. Unique diagnostic and therapeutic roles of porphyrins and phthalocyanines in photodynamic therapy, imaging and theranostics. Theranostics. 2012;2:916-66.

[35] Li R, Zheng K, Hu P, Chen Z, Zhou S, Chen J, et al. A novel tumor targeting drug carrier for optical imaging and therapy. Theranostics. 2014;4:642-59.

[36] Ganguly NC, Mondal P. Mild, Efficient, and greener dethioacetalization protocol using 30% hydrogen peroxide in catalytic combination with ammonium iodide. Synthetic Commun. 2011;41:2374-84.

[37] Lee CS, Park W, Park SJ, Na K. Endolysosomal environment-responsive photodynamic nanocarrier to enhance cytosolic drug delivery via photosensitizer-mediated membrane disruption. Biomaterials. 2013;34:9227-36.

[38] Li Y, Liu R, Yang J, Ma G, Zhang Z, Zhang X. Dual sensitive and temporally controlled camptothecin prodrug liposomes codelivery of siRNA for high efficiency tumor therapy. Biomaterials. 2014;35:9731-45.

[39] Zhen Z, Tang W, Guo C, Chen H, Lin X, Liu G, et al. Ferritin nanocages to encapsulate and deliver photosensitizers for efficient photodynamic therapy against cancer. Acs Nano. 2013;7:6988-96.

[40] Zhang CL, Zhou ZJ, Zhi X, Ma Y, Wang K, Wang YX, et al. Insights into the distinguishing stress-induced cytotoxicity of chiral gold nanoclusters and the relationship with GSTP1. Theranostics. 2015;5:134-49.

[41] Ho CJH, Balasundaram G, Driessen W, McLaren R, Wong CL, Dinish U, et al. Multifunctional photosensitizer-based contrast agents for photoacoustic imaging. Scientific reports. 2014;4:5342.